

Refractory Corrosion Mechanisms in a Novel High Carbon Ferromanganese Production Furnace

D. GREGUREK,^{1,5} C. WENZL,² D. KREUZER,² A. SPANRING,²
M. KIRSCHEN,² D. ZEELIE,³ and J. GROENEWALD⁴

1.—RHI AG; TC Leoben, Magnesitstrasse 2, Leoben 8700, Austria. 2.—RHI AG, Wienerbergstrasse 9, Vienna 1100, Austria. 3.—74 Queen Street, Irene Proper, Centurion, South Africa. 4.—Roger Dyason Road, Pretoria West 0183, PO Box 9229, Pretoria 0001, South Africa. 5.—e-mail: dean.gregurek@rhi-ag.com

The present paper presents the refractory design for a novel HCFeMn smelting furnace that, other than standard submerged arc furnaces, allows the processing of fine ores. A combination of basic and non-basic materials, comprising bricks, castables and ramming was chosen, under consideration of the unique furnace design and process conditions. Post-mortem investigations on refractory samples from the different furnace zones were carried out and provided information about the main wear mechanism. Additionally, investigations of the process slag and metal were carried out both practically and theoretically using thermodynamic calculations, to better understand the corrosion phenomena observed in the post mortem samples.

INTRODUCTION

Today's main share of the worldwide high-carbon ferromanganese (HCFeMn) production is realized in submerged arc furnaces (SAF) by carbo-thermic reaction of manganese ores; blast furnaces (BF) are also used, but with a decreasing share.^{1–5} Generally, two different industrial practices for the SAF production are used, namely discard slag practice and high-MnO-slag practice or duplex method, as the second one is typically connected to a combined silico-manganese (FeSiMn) production. The main difference between the two process variants is slag basicity, which is a crucial parameter for manganese reduction besides the CO partial pressure.⁶ The operation of HCFeMn production commonly follows the high-MnO slag practice. The produced metal typically contains around 78% Mn and 7% C, and the slag around 40% MnO.¹

In the SAF process, the feed mixture composition is typically constrained by the need to conduct electricity through the highly resistive slag layer where the energy is mainly dissipated. The energy input and penetration depth of the electrodes depend on the electrical conductivity of the burden and slag, which in turn is determined by their chemical composition. Conditioning of the feed mixture is necessary to adjust the slag chemistry

and to achieve appropriate physical properties for the furnace operation. The electrical conductivity of slags depends highly on their structure and hence their chemical composition. Slag components can be divided in network-forming oxides (e.g., SiO₂ forming a network with SiO⁴⁻ anions in manganese silicate slag) and network-breaking oxides (e.g., MnO, CaO and MgO forming Mn²⁺, Ca²⁺ and Mg²⁺ cations). In the crystalline silica, each Si atom is surrounded by 4 oxygen atoms, where each oxygen atom is shared by 2 neighboring Si atoms. In the molten state, the structure is distorted and network-breaking oxides connect with the silicate anions, which changes the network into complex rings and chains. The slag's electrical conductivity depends on the movement of the cations through the network and is influenced by two main factors: the degree of polymerization (number of connected SiO⁴⁻ anions) and the size and concentration of the cations. The conductivity decreases with increasing polymerization and increases with higher cation concentrations and smaller cation sizes. Thus, substituting SiO₂ by the mentioned basic oxides (i.e., MnO, CaO, and MgO) will increase the electrical conductivity of the slag.¹ Lumpy feed (i.e., ore, sinter and reductive feed) is required to guarantee sufficient gas permeability for an even gas distribution through the burden in the SAF.



Fig. 1. Photo of the FeMn furnace during tapping.

Close packing of material fines in the SAF promote the risk of calcine bridge formation and gas eruptions, which decrease the furnace efficiency.^{1,2}

The novel AlloyStream™ process was specifically designed to handle ore fines in a single step production unit. The process was developed over almost a decade from bench scale to a pilot plant with a furnace of 5.3 m in diameter and a production capacity of 8000 tons/year. Figure 1 shows the ferromanganese pilot furnace during tapping. The energy input into the furnace is realized by two different sources, namely a coreless inductor and an oxygen-enriched combustion. The furnace is fed through the roof with a mixture of ore, coal and fluxes, which form heaps on the metal bath surface. The space above the heaps is used as combustion zone, where natural gas, coal volatiles and reaction gases are burned by the introduction of oxygen-enriched air via lances. The released energy is transferred to the feed material via radiation.⁵

The Alloystream™ process has several advantages compared to the standard SAF route.² It is more flexible in terms of the used feed material and quality, as the energy input can be controlled independently from the slag chemistry. Slag conditioning for a SAF operation requires a compromise between a proper electrical conductivity and a basicity that enables a sufficient degree of manganese reduction. In contrast, the slag basicity in the newly developed process can be controlled independently from the slag's electrical conductivity. The SAF operation requires proper sizing of the raw materials, which is realized by an agglomeration process of the ores and concentrates by sintering, pelletizing or briquetting. This process step comes with an additional energy demand and capital investment. Due to the carbo-thermic reaction, a CO-rich gas is produced, which in the case of a SAF operation has to be collected and burned in an energy recovery unit to increase the energy efficiency of the process. Therefore, it is essential to seal the furnace roof to avoid or reduce ingress of air. In the combustion zone of the new process, the

energy release due to CO oxidation directly contributes to the energy supply, hence ingress of air is of minor importance and additionally the utilization of the CO gas combustion is more efficient.¹⁻³ The electricity consumption of a well-established SAF route and the novel Alloystream™ process pilot plant show similar values: typical values for the high-MnO slag practice SAF operation are in the range of 2200–3500 kWh/t alloy^{3,7} and the latest evolution of the Alloystream™ pilot plant consumes about 2300–2900 kWh/t alloy² depending on the used raw material composition.

RHI AG was assigned as exclusive key supplier of the furnace refractory lining and developed the refractory concept in close collaboration with Exxaro AlloyStream™. In the development of the Exxaro AlloyStream™ process, several campaigns were completed on pilot and demonstration plant scale.⁸ Four ferromanganese campaigns, as well as one ferronickel and one steel campaign were completed in the pilot plant furnace with 2.5 m diameter between 2003 and 2009. For process scale-up, a 5.3-m-diameter demonstration furnace was constructed (Fig. 1) and used to complete two HCFeMn campaigns between 2012 and 2014, operated on a semi-commercial base. During the last campaign, spanning 11 months, 5014 tons of HCFeMn were tapped from the demonstration furnace. The design and selection of the refractory material were based on thorough investigations of the refractory wear mechanism in small-scale laboratory experiments complemented by detailed analysis of the refractory corrosion phenomena of the different furnace campaigns.^{9,10} Since the AlloyStream™ process shows fundamental differences to the SAF process, different requirements evolved in terms of the refractory selection. The refractory lining design had to be adapted to the special demands of the different furnace zones.

Figure 2 depicts the schematic of the production furnace (copper coolers are not indicated). From the top, a raw material blend was fed onto a liquid metal bath forming piles of pre-reacted material. The material was heated from above mainly by thermal radiation which was generated by burning combustibles with enriched air. The combustibles consisted of natural gas, coal volatiles, coal carbon, and gaseous reaction products emanating from the packed bed. The final reaction and smelting of the feed mixture was realized with a bottom inductor, which transferred energy to the metal bath and consequently to the material heaps. The reaction temperature of the material mixture was in the range of 1400°C. The AlloyStream™ process intended to utilize FeMn ores without compositional constraints and flux additions, hence no excessive slag adjustments were made. Slag and metal alloy were tapped through one tap hole and tilting of the furnace. The design temperatures of metal bath and combustion zone were in the range of 1550°C and 1600°C, respectively.⁸

PROCESS PARAMETERS AND FURNACE LINING

Process Parameters

The feed material consisted of a mixture of fine oxidic Fe-Mn ore, coal and slag conditioner (silica sand). Two ore types (Mamatwan and Wessels ore, grain sizes 3–10 mm) with different CaO content and Fe/Mn ratio were blended to obtain the desired metal ratio in the final product. The basic ore contained a high amount of fine dust material (<1 mm). The ore mixing ratio varied between 43% and 80%.⁸ The chemical compositions of the two ore types are presented in Table I.

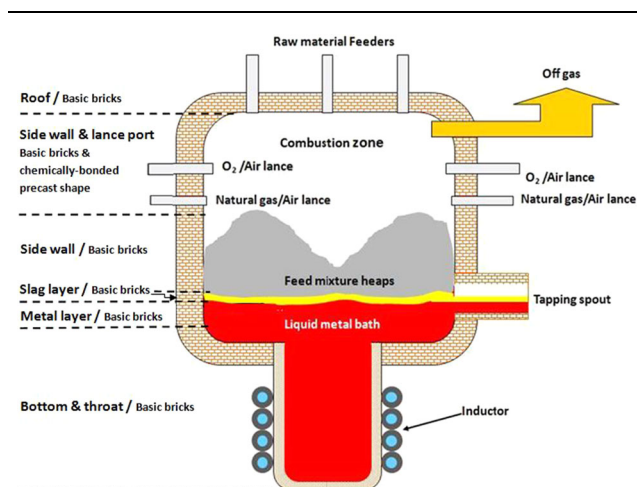


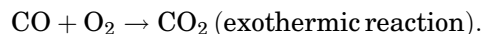
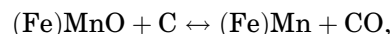
Fig. 2. AlloyStream™ process—schematic.⁵ The position of the copper coolers is not shown.

Table I. Ore bulk chemical composition (wt.%)²

	Mamatwan	Wessels
<i>Ore composition</i>		
SiO ₂	5.04–6.45	2.00–4.07
Al ₂ O ₃	0.22–0.44	0.39–0.46
FeO ^a	5.7–7.6	18.8–26.2
TiO ₂	0.01–0.02	0.02–0.03
CaO	12.80–15.00	3.99–5.61
MgO	3.19–3.69	0.50–0.65
K ₂ O	0.08–0.12	0.02–0.13
MnO ^b	44.7–49.1	52.9–58.7
P	0.02–0.04	0.04–0.08
Ba	0.05–0.11	0.49–0.81
Moisture	0.12–0.70	0.09–0.70
Total	76.4–76.9	86.6–93.1
B2	2.9–2.6	1.4–2.0
B3	2.8–3.3	1.5–2.2
Mn/Fe	6.4–8.6	2.2–3.0

B2 = pct CaO/pct SiO₂; B3 = (pct CaO + pct MgO)/pct SiO₂.^aTotal iron expressed as FeO. ^bTotal manganese expressed as MnO.

The total feed rate was distributed over multiple feedports. The feed material mix fell towards the furnace bottom by gravity (no blowing). The following reactions occurred:



Additionally, a natural gas rich in CH₄ was used to generate sufficient energy for the combustion and reduction of the oxidic ore.

Multiple fuel lances and air/oxygen lances were located in the combustion zone directly below the raw material feed ports. The theoretical flame temperature could reach up to 2300°C; however, the actual flame temperature was strongly dependent on fuel gas composition and combustion air ratio.

The density of the FeMn metal is 5.5¹¹–5.6¹² g/cm³. The furnace inside (i.e., combustion zone and slag line) is shown in Fig. 3.

Furnace Lining

In most cases, FeMn furnaces are lined with carbon materials, due to the similarity of Mn oxide to the oxides in refractory materials and subsequent possible reactions, namely refractory corrosion.^{13,14} Besides the chemical composition of the process phases and process conditions (e.g., temperatures, atmosphere, flow conditions), the thermal profile of the furnace and possible cooling equipment has to be considered in the material selection and lining design.¹⁵ The aim for the AlloyStream™ process was to develop a novel lining solution based on non-carbon materials. After initial theoretical considerations and laboratory-scale tests at RHI's Technology Center Leoben (TCL), a combination of basic and non-basic bricks, castables and rammings was defined that were subsequently used for refractory engineering.

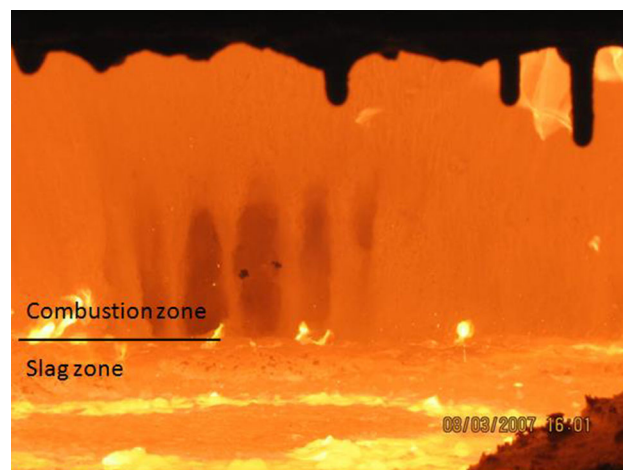


Fig. 3. View from the inspection door at the north furnace side. Slag line and combustion zone.

The refractory selection was based on results from preliminary laboratory-scale studies performed at RHI's TCL, namely cup tests of different refractory materials in contact with FeMn slag and metal. During the first pilot plant furnace campaigns, the most promising materials from the cup tests, as well as different refractory designs, were tested and later implemented in the demonstration furnace. Magnesia-based materials were the first choice, because of their high thermal conductivity in comparison with other refractory materials. The high thermal conductivity was a decisive factor and required to guarantee a frozen material layer as refractory protection ("freeze lining") in combination with the strong furnace cooling. The very limited target carbon content in the metal did not allow for the use of a carbon lining.

The furnace bottom (hearth) and the throat consisted of two horizontal layers of basic bricks. The sidewall of the furnace was divided into three zones (i.e., metal zone, slag zone and combustion zone) and was also lined with high-quality basic bricks, the combustion zone with a spinel-containing material for better thermo-shock resistance. Copper cooling elements were used to enable the formation of a protective frozen layer on the basic bricks in the slag zone, which is the most critical area regarding chemical attack. A conductive carbon ramming was used between the shell and the refractory bricks to guarantee an effective heat transfer of the channel cooling system. Non-basic bricks of different alumina content and insulating bricks were used in the safety lining in the bottom and sidewalls, depending on the thermal requirements. A basic ramming was used for leveling between working and safety lining. High-quality basic bricks were used for the tap hole. Due to the multiple openings for feed ports and offgas duct, it was decided to use a castable in the furnace roof.

ANALYTICAL PROCEDURE

As mentioned above, several campaigns were carried out in the furnace. Afterwards, the furnace was stopped and refractory samples were taken from the different furnace areas to study the refractory conditions and wear mechanism (i.e., post-mortem studies) at RHI's TCL. The results should provide information about the suitability of the chosen materials for the novel process and possible optimization potential.

Generally, every post-mortem study at the TCL starts with a visual inspection carried out on the brick cross-section followed by selection of samples for chemical analysis and detailed mineralogical investigation. The chemical analysis was carried out using x-ray fluorescence analysis (XRF) (Bruker S8 TIGER). The mineralogical investigation was performed on polished sections using a reflected light microscope and a scanning electron microscope

(SEM) (JEOL JSM-6460) combined with an energy-dispersive and wave-dispersive x-ray analyser. Additionally, x-ray diffraction (XRD) (Bruker D8 ADVANCE) was used for slag phase analysis. The measurement of the slag melting point according to DIN 51730¹⁶ was carried out using a heating microscope.

RESULTS AND DISCUSSION

Chemical corrosion of refractories in contact with process phases (i.e., slag, metal, gas) is an essential factor regarding lining wear and consequently duration of furnace campaigns.^{9,10} Hence, it is important to study the process phases that are in contact with the refractories to get a better understanding of their composition and melting behavior, as well as the detected corrosion phenomena in the post mortem samples.¹⁷

Slag and Metal Analyses

The average chemical analysis including XRD of the slag is shown in Table II. The slag represented a basic, manganese-rich calcium silicate slag. The MnO content was up to 26 wt.%.

According to the microscopical investigation and XRD, the main slag components were Ca-Mg-silicate merwinite ($\text{Ca}_3\text{MgSi}_2\text{O}_8$), Ca-Al-silicate gehlenite ($\text{Ca}_2\text{Al}_2\text{SiO}_7$), and Mn-Mg-oxide of type manganosite (MnO).¹⁸ At the rims of the merwinite, but also in the matrix due to the high MnO-content, a Ca-(Mg)-Mn-silicate of type glauchochroite ($(\text{Ca},\text{Mn})_2\text{SiO}_4$) also formed (see Table II). Minor amounts of Mn-sulfide (type hauerite, MnS_2), idiomorphic Mg-Mn-Al-spinel (spinel-galaxite mixture), as well as sulfur- and chlorine-containing Na-Ca-Ba-Mg-Mn-Al-Ti-Zr-silicatic glassy phase were additionally detected by SEM. The determined slag melting point by heating microscope was 1365°C.

Additionally to the investigation with the heating microscope, thermodynamic calculations with FactSageTM software¹⁹ were carried out in order to determine the slag liquidus and the solidus temperature. Gehlenite, merwinite (Mn,Mg)O-phase, spinel and oxidic liquid were determined as stable phases, which was consistent with the mineralogical investigation and the chemical analysis. The calculated liquidus temperature was 1354°C and therefore comparable with the results obtained with the heating microscope. At this temperature, merwinite was the first phase that formed, followed by MnO-phase at 1151°C and gehlenite at 1054°C. The last phase crystallizing from the melt was spinel (galaxite) at 1042°C. The calculated solidus temperature was 785°C. Due to database limitations for complex solutions, the calculated crystallization temperature and amounts of (Mg,Mn)-oxide and Mn-spinel may be underestimated, as only stoichiometric MnO and galaxite MnAl_2O_4 were considered.

Table II. Average slag analysis received from AlloyStream™ (wt.%) and XRD-analysis

<u>MgO</u>	<u>Al₂O₃</u>	<u>SiO₂</u>	<u>CaO</u>	<u>TiO₂</u>	<u>MnO</u>
7.56–8.25	7.94–9.10	23.7–26.4	31.2–34.5	0.42–0.44	18.1–25.7
Merwenite		Ca ₃ Mg(SiO ₄) ₂		10–50%	
Gehlenite		Ca ₃ Al ₂ (SiO ₇)		10–50%	
Glaucochroite		(Ca,Mn) ₂ SiO ₄		5–10%	
Manganosite		MnO		2–5%	

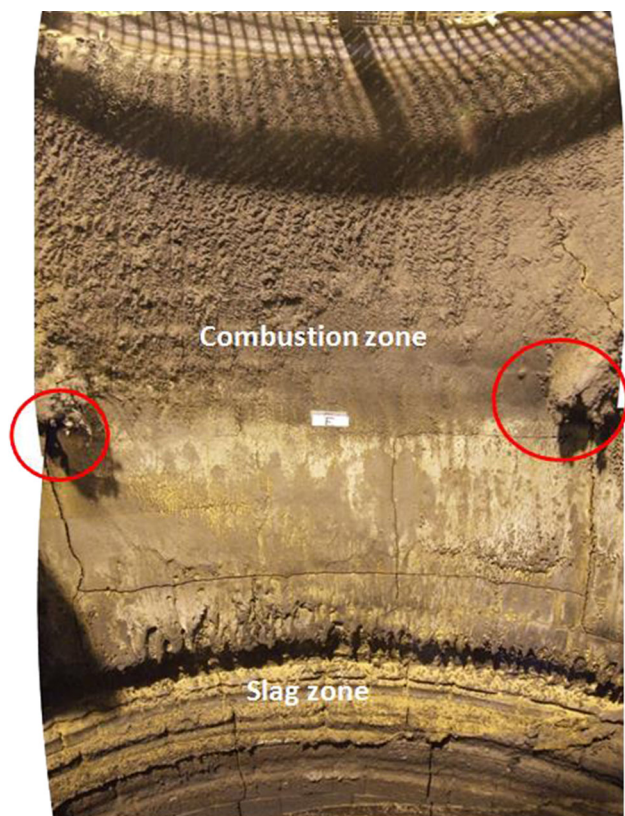


Fig. 4. View of the combustion and slag zone at the eastern furnace side. Severe corrosion of the refractory in the slag zone. Formation of massive build ups at the lance ports (circles).

According to the SEM investigation and the EDX-analysis, the investigated metal sample represented a FeMn-alloy (26 wt.% Fe and 74 wt.% Mn) with some minor content of Si, P and S. The melting point of the FeMn-alloy determined by the heating microscope was 1330°C.

Post-mortem Study

Evaluation of the Refractory Lining and Sampling

During the furnace inspection, the lower furnace areas (bottom, throat and metal bath zone) showed only minor wear. The brick lining was in good condition showing nearly original brick thicknesses and minor penetration of FeMn and slag into the brick joints. As described above, several campaigns



Fig. 5. Oxygen lance. Massive build up and wash outs of the refractory side wall below the build up.

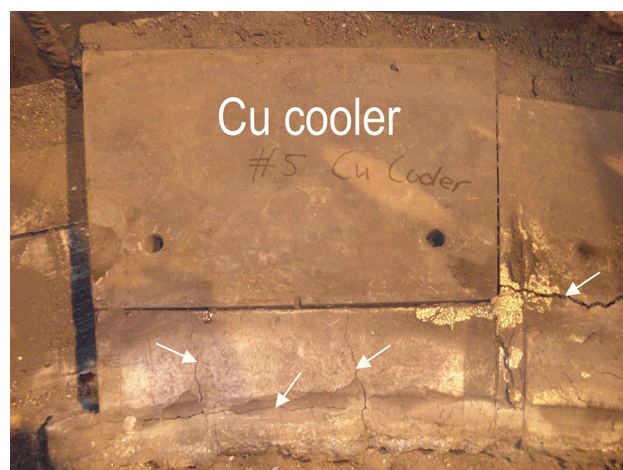


Fig. 6. Furnace side wall (slag line). Brick in front of the copper cooler showing crack formation (arrows).

were carried out, and the refractory samples were taken from the last (HCFeMn) demonstration furnace campaign.

The highest refractory wear was observed in the slag zone (see Fig. 4) and tap hole area. On the lances—particularly on the fuel gas lances—a massive dark-coloured build-up with a high content of Fe-Ni-Mg-Al-Si-oxide had formed (Figs. 4 and 5).

The measured residual thickness of the brick lining in the slag zone (in front of the copper cooling element) was on average 90 mm. Especially in front of the copper cooler, a massive crack formation was detected, which had resulted from the thermal shock during furnace shutdown and cool-down (Fig. 6).

Five representative brick samples from each furnace section were taken for post-mortem investigation (Fig. 7a–e):

- Sample 1 (furnace bottom, floor lining, Fig. 7a) represents a magnesia-spinel brick which is based on magnesia and MA-spinel;
- Sample 2 (furnace side wall, slag zone, Fig. 7b) and sample 3 (furnace side wall, combustion zone, Fig. 7c) represent dense magnesia bricks;
- Sample 4 (furnace side wall, combustion zone lance port, Fig. 7d) represents a chemically bonded precast shape based on magnesia;

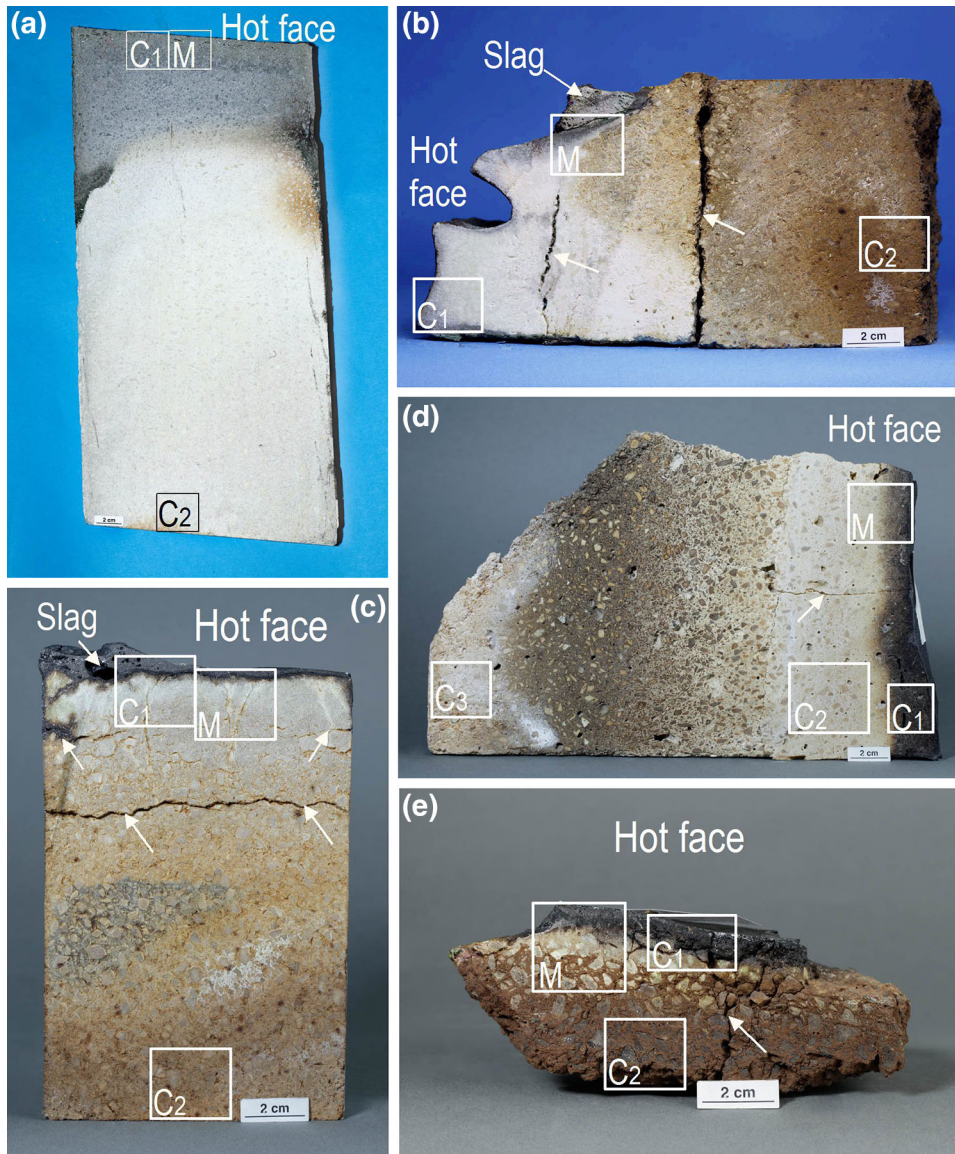


Fig. 7. (a) Furnace bottom (floor lining). Sample 1. Original brick thickness. The dark-colored area represents the infiltrated brick microstructure. The white brick colour is due to reduction phenomena. (b) Furnace side wall (slag zone). Sample 2. Slag coating on the immediate brick hot side. Groove on the hot side was caused by slag corrosion. Slag is partly sticking to the brick hot side. Crack formation (arrows). Cold end of the refractory broken during furnace demolition. (c) Furnace side wall (combustion zone). Sample 3. The immediate brick hot side is covered with slag coating. Below the slag coating: infiltrated brick microstructure. The infiltration depth is up to approximately 30 mm from the hot side. Horizontal cracks (arrows). (d) Furnace side wall (combustion zone, lance port). Sample 4. Dark-colored reaction zone on the immediate brick hot side. Below the reaction zone: deeply infiltrated microstructure of the basic precast shape. The infiltration depth is up to approximately 90–100 mm from the hot side. (e) Furnace roof. Sample 5. Thin reaction zone on the immediate hot face (dark color). Infiltration depth < 1 mm. Vertical crack (arrow). In (a–e), samples for chemical analyses (C₁–C₃). Polished sections for mineralogical investigation (M).

- Sample 5 (furnace roof, Fig. 7e) represents a phosphorous-bonded basic castable based on magnesia.

The sampling positions for chemical analyses (Table III) and mineralogical investigation are marked on the cross-section of the refractory samples. The detailed analyses (i.e., macroscopical, chemical and mineralogical) of the samples are described in the following sections. The chemical composition of unused refractories is shown in Table IV.

Furnace Bottom (Floor Lining): Sample 1 The brick sample showed nearly original thickness with 400 mm. The macroscopically visible infiltration depth was up to approximately 140 mm from the hot side (dark-colored area in Fig. 7a).

According to the chemical analysis the brick hot side was highly enriched with MnO (up to 11 wt.%) and Fe-oxide (Table III). Increased CaO and SiO₂ content originating from slag infiltration was also determined.

In the infiltrated brick area (0–25 mm from the hot side), a highly degenerated microstructure was observed.

The following microstructural changes can be summarized:

- Extreme elongation of the periclase crystals (up to several mm in size) towards the thermal gradient (Fig. 8a). This phenomena is called epitaxial crystal growth.¹⁰ The MnO content within the magnesia is in the range between 8 and 13 wt.%. The typical ceramic microstructure with coarse grains and fines, as shown in Fig. 8b for the not-infiltrated brick, was completely lost.
- Infiltration of the microstructure with FeMn.

The increased CaO and SiO₂ content are a proof for slag penetration: slag penetrated into the brick microstructure only in the first few mm from the hot face and after the metal tapping. The furnace bottom (floor lining) was not cooled and due to high metal wettability the first 140 mm of the 400-mm-

Table III. Chemical analysis of used basic brick (samples 1–5) out of the ferromanganese furnace (wt.%)

Sample	Sampling/Description	Na ₂ O	MgO	Al ₂ O ₃	SiO ₂	P ₂ O ₅	SO ₃	CaO	TiO ₂	MnO ^a	Cr ₂ O ₃	Fe ₂ O ₃ ^b
1	Hot side (0–25 mm) (C1)		78.2	5.0	2.0			2.0		10.7		2.0
	Cold end (C2)		90.5	7.5	0.3		0.1	0.9				0.6
2	Hot side (0–25 mm) (C1)		91.3	2.0	1.8			3.0		0.5		0.9
	Cold end (C2)		96.9	0.1	0.6			1.0				0.5
3	Hot side (Slag coating, 0–10 mm) (C1)		28.5	17.8	10.0			3.7	0.5	30.1		8.8
	Hot side (10–30 mm) (C2)		87.1	1.3	5.4	0.1		4.4		0.8		0.5
	Cold end (C3)		97.0	0.1	0.5		0.9	0.9				0.4
4	Hot side (0–20 mm) (C1)		65.9	5.5	9.3	0.1		3.1	0.2	12.6		2.9
	Hot side (30–60 mm) (C2)	1.2	79.6	5.0	4.8	3.7		5.0	0.1	0.1		0.4
	Cold end (C3)	1.2	87.6	6.9	0.4	2.1		1.1		0.1		0.5
5	Hot side (0–15 mm) (C1)	0.2	65.6	2.7	5.2	0.4		2.5	0.1	17.3	1.5	4.4
	Cold end (C2)	0.8	92.6	0.2	0.6	1.2	0.4	1.2		0.1	2.1	0.7

^aTotal manganese expressed as MnO. ^bTotal iron determined as Fe₂O₃.

Table IV. Chemical analysis of unused basic brick (samples 1–5)

Sample	MgO	Al ₂ O ₃	SiO ₂	P ₂ O ₅	CaO	Cr ₂ O ₃	Fe ₂ O ₃ ^a
1	90.8	7.5	0.3		0.8		0.5
2	98.0	0.1	0.3		0.8		0.1
3							
4	91.0	5.0	0.2	1.7	1.1		0.2
5	93.0		0.5	1.3	1.8	1.9	0.4

^aTotal iron determined as Fe₂O₃.

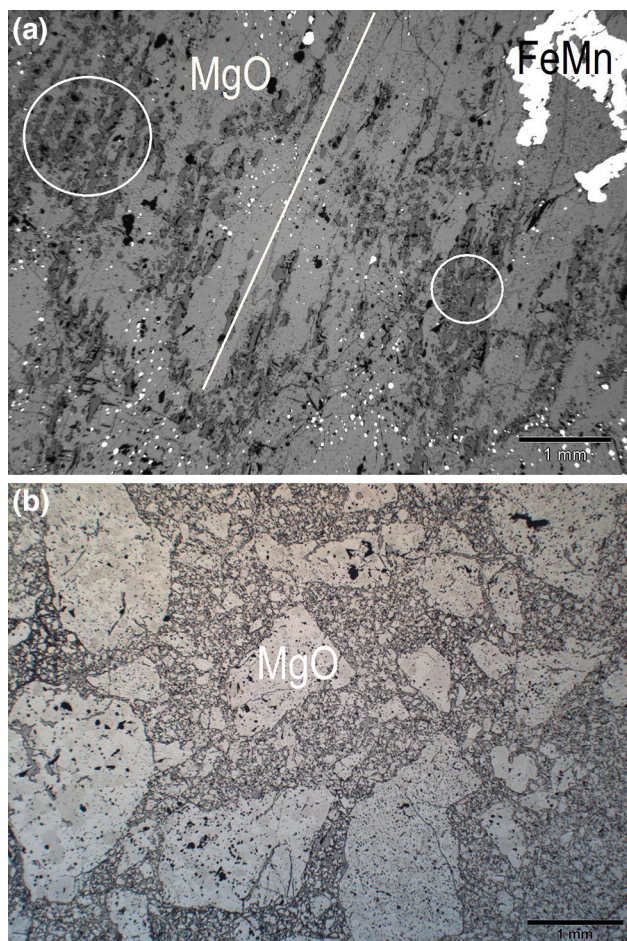


Fig. 8. (a) Furnace bottom (floor lining). Sample 1. Immediate brick hot side. Extreme elongation of periclase crystals (epitaxial crystal growth) towards the thermal gradient (lines). Magnesia (MgO). Ferromanganese (FeMn). Coarse pores formed due to severe degeneration of the brick microstructure (circles). (b) For comparison to Fig. 8a, original microstructure of the not-infiltrated brick at same magnification. Magnesia (MgO).

long brick were infiltrated with the FeMn. After the metal infiltration, the subsequent oxidation of the metal to Mn- and Fe-oxide, i.e., after furnace tapping, resulted in incorporation of both cations into magnesia by diffusion and formation of solid solution.

Based on the observed chemical analyses and determined MnO content in the magnesia, the liquidus temperature calculated with FactSageTM software was $>2000^{\circ}\text{C}$ (Fig. 9a). At this temperature, the $(\text{Mg,Mn,Ca})\text{O}_{\text{ss}}$ for MnO-enriched magnesia was the first phase formed. Assuming a local equilibrium of the analyzed area around the magnesia grains with MnO-bearing infiltrate, the analyzed MnO content of the $(\text{Mg,Mn,Ca})\text{O}_{\text{ss}}$ corresponded to thermo-chemical equilibrium temperatures between 1930°C and 1960°C (Fig. 9b). The latter indicated correspondingly high process temperatures and a consequently strongly overheated slag that promoted chemical corrosion effects.

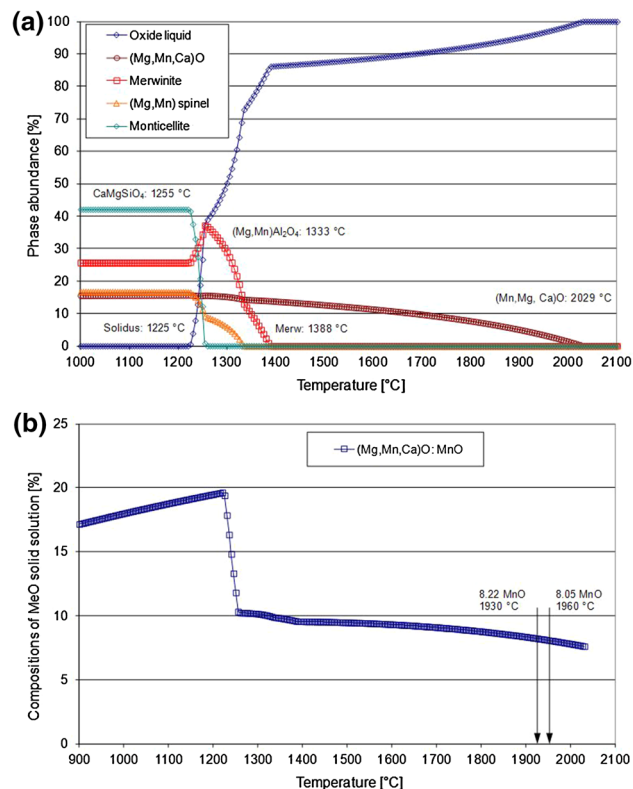


Fig. 9. (a) Furnace bottom (floor lining). Sample 1. FactSageTM calculation showing liquidus temperature $>2000^{\circ}\text{C}$. (b) Furnace bottom (floor lining). Sample 1. FactSageTM calculation. The thermo-chemical equilibrium temperatures is 1930°C and 1960°C for the local equilibrium of the analyzed area around the magnesia grains with MnO-bearing infiltrate.

Furnace Sidewall (Slag Zone): Sample 2 This brick sample was taken from the area directly in the front of the copper cooling element. Due to severe slag corrosion, a massive groove had formed (Fig. 7b). The brick hot side had declined and was partly covered with slag coating. On the cross-section, the macroscopically visible infiltration depth was up to 100 mm from the hot side. In the infiltrated brick microstructure, but also at the interface to the not-infiltrated microstructure, cracks had formed parallel to the hot side. The rough surface at the brick cold end indicated that the refractory was broken during demolition and sampling.

The chemical analysis of the infiltrated brick area at the hot side showed a significantly increased content of CaO, Al_2O_3 and SiO_2 (Table III).

The results of the mineralogical investigation carried out on the refractory hot side can be summarized as follows:

- On the immediate hot side and below the slag coating, a 2-mm-thin reaction zone was observed (Fig. 10a). The latter consisted of magnesia highly enriched with MnO, MnO-rich monticellite, idiomorphic MnO-rich MA-spinel and FeMn.

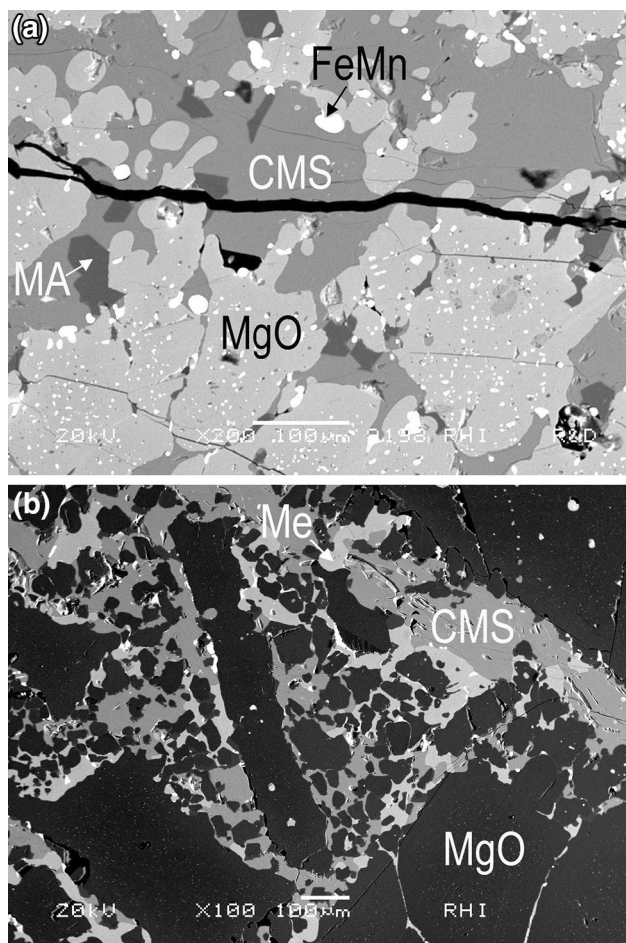


Fig. 10. (a) Furnace side wall (slag zone). Sample 2. Immediate brick hot side. Detail of the reaction zone. MnO-rich monticellite (CMS). Magnesia highly enriched with MnO (MgO)—formation of MgO–MnO solid solution. Idiomorphic MnO-rich MA-spinel (MA). Ferromanganese (FeMn). (b) Furnace side wall (slag zone). Sample 2. Approximately 5 mm from hot side. Infiltrated brick microstructure. Partly corroded magnesia (MgO). The magnesia is highly enriched with MnO (up to 35 wt.%), resulting in formation of MgO–MnO solid solution. Mn-rich monticellite (CMS). Merwinite (Me).

- Below the reaction zone in the infiltrated brick microstructure, severe corrosion of the main brick component magnesia took place. The main reaction products included MnO-bearing Ca-Mg-silicates of monticellite and merwinite ($\text{Ca}_3\text{Mg-Si}_2\text{O}_8$) type (Fig. 10b).

Furnace Side Wall (Combustion Zone): Sample 3

The residual brick thickness was 150 mm. On the cross-section of the refractory, horizontal cracks were macroscopically visible (Fig. 7c). The immediate brick hot side was covered with an approximately 10-mm-thick slag coating.

The chemical analysis of the slag coating is shown in Table III. The brick hot side below the slag coating was highly enriched with CaO and SiO_2 (see Table III). An elevated Al_2O_3 and MnO were also determined.

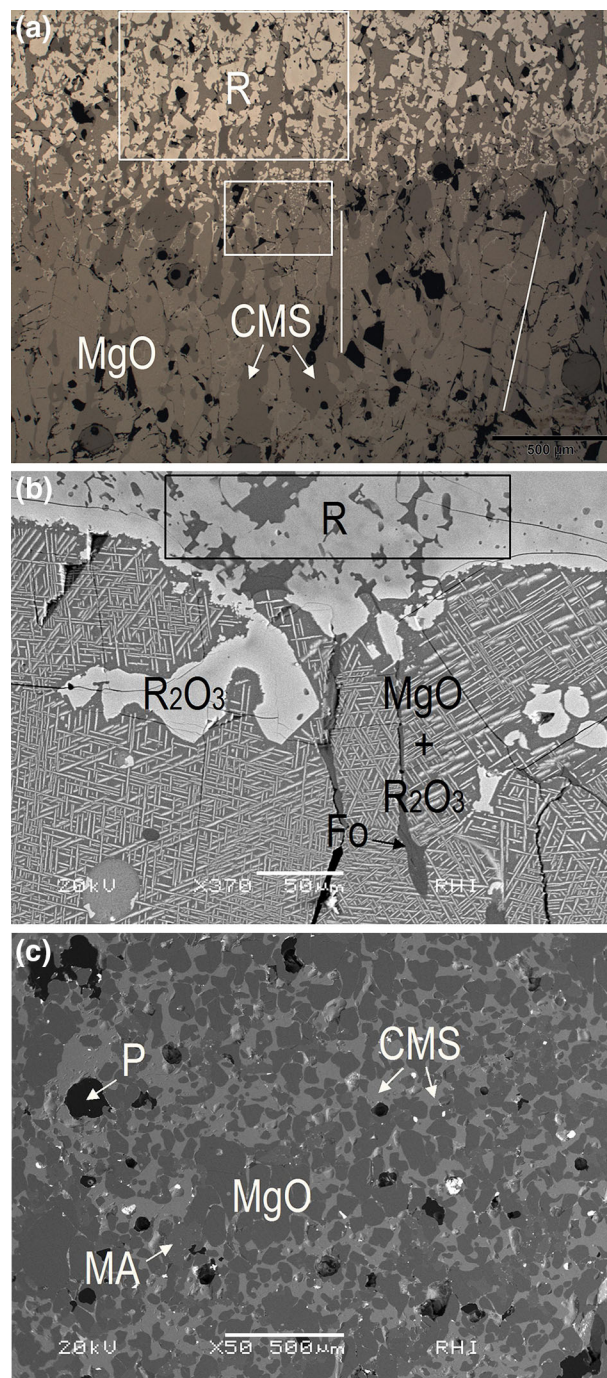


Fig. 11. (a) Furnace side wall (combustion zone). Sample 3. Immediate brick hot side with reaction zone (R). Below that degenerated and infiltrated brick microstructure with elongation of periclase crystals (lines). Corroded magnesia (MgO). Monticellite (CMS). (b) Furnace side wall (combustion zone). Sample 3. Detail (rectangular) from Fig. 11a. Immediate brick hot side with reaction zone (R). Below the reaction zone and within infiltrated brick microstructure: magnesia highly enriched with MnO (MgO), i.e., formation of MgO–MnO solid solution. The MnO content is up to 40 wt.%. The lamellae in the MgO and idiomorphic light phase crystals represent “ R_2O_3 -oxides” consisting mainly of Fe_2O_3 and Mn_2O_3 which precipitated and formed after furnace cool-down. Mn-rich forsterite (Fo). (c) Furnace side wall (combustion zone). Sample 3. Approximately 20 mm from hot side. Infiltrated brick microstructure. Corroded magnesia (MgO). The magnesia rims are enriched with MnO. Mn-rich monticellite (CMS). MA-spinel (MA). Pore (P).

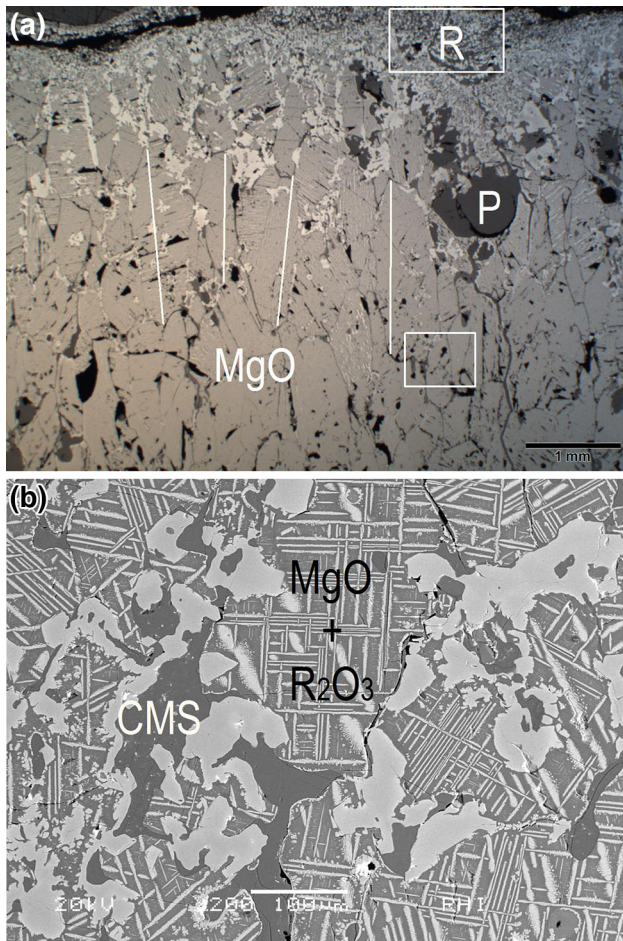


Fig. 12. (a) Furnace side wall (combustion zone, lance port); Sample 4. Reaction zone (R). Below the reaction zone severely degenerated brick microstructure with crystal growth and massive elongation of the periclasite crystals (lines). Formation of coarse pores (P). (b) Detail (rectangular) from Fig. 12a. Magnesia (MgO) with R_2O_3 -oxides precipitations. Mn-rich monticellite (CMS).

The microstructural degeneration below the reaction zone was very similar to the previously described samples 1 and 2, i.e., elongation of periclasite crystals, infiltration of the microstructure and corrosion of magnesia, as well as enrichment of the magnesia with MnO and formation of MgO-MnO solid solution (see Fig. 11a–c).

Furnace Sidewall (Combustion Zone, Lance Port): Sample 4 The thickness of the sample 4 was 135–270 mm. The infiltration depth was up to approximately 100 mm from the hot side (Fig. 7d). A vertical crack in the infiltrated brick microstructure was visible.

According to the chemical analyses, the brick hot side (0–60 mm) was highly enriched with CaO and SiO_2 (Table III). Additionally in the first 20 mm from the hot side, a highly increased content of MnO and Fe-oxide was determined.

Microscopically, the immediate brick hot side was covered with a 1- to 2-mm thin reaction zone. Similar to the previously described samples, a

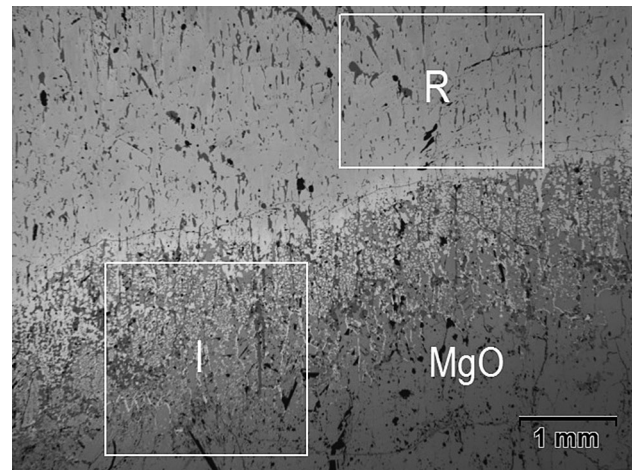


Fig. 13. Furnace side roof. Sample 5. Immediate brick hot side with reaction zone (R). Below the reaction zone: degenerated and infiltrated brick microstructure (I). Corroded magnesia (MgO).

severely degenerated microstructure with extreme elongation of MnO-rich periclasite crystals combined with formation of coarse pores was observed below the reaction zone (see Fig. 12a). Due to a high enrichment of the magnesia with manganese- and iron-oxide, precipitations of R_2O_3 -oxide type had formed (Fig. 12b). Adjacent to the reaction zone in the infiltrated brick microstructure, a Mn-rich monticellite and a MA spinel were formed due to corrosion of sintered magnesia.

Furnace roof: Sample 5 The small refractory sample of used basic castable had thicknesses of 20–30 mm. The infiltration of the microstructure visible on the cross-section was up to approximately 5 mm from the hot side (Fig. 7e). The latter was also confirmed by the chemical analysis that showed an increased content of MnO, CaO, Fe-oxide, Al_2O_3 and SiO_2 within this brick area (Table III).

According to the mineralogical investigation, the immediate brick hot side was covered with a thin reaction zone (Fig. 13). Below the reaction zone and within the first 2 mm from the hot face, there was a severe degeneration of the microstructure. This was mainly caused by infiltration and corrosion of both magnesia and the bonding phase. The main reaction products were monticellite and Mn-rich forsterite. The corrosion of the bonding phase resulted in formation of phosphorous-containing Na-Ca-K-Mg-silicate. Within this area, the magnesia was highly enriched with MnO (up to 40 wt.%, MgO-MnO solid solution). Crack formation parallel to the hot face (partly softening cracks) was also observed in the infiltrated microstructure.

CONCLUSION

The slag and metal were analyzed and also compared to theoretical thermodynamic calculations. The evaluation of the results indicated a

strongly overheated slag that promoted chemical refractory corrosion. It can be assumed that the metal phase was also overheated, resulting in deeper infiltration of the refractories.

The main wear phenomena observed in the investigated samples from the ferromanganese furnace are summarized in the following:

- The main refractory wear was predominantly continuous wear due to hot erosion. Also, discontinuous wear due to spalling (as a consequence of infiltration and temperature variations) contributed to refractory damage.
- All refractory samples suffered from a high chemical attack in combination with high thermal load. The thermodynamic calculations with FactSage™ indicate temperatures >1800°C. The chemical slag attack resulted in infiltration of the microstructure and severe corrosion of the main brick components, mainly MgO. The main reaction products included MnO-rich monticellite and forsterite, as well as MA-spinel. Additionally, the high enrichment of the magnesia with MnO resulted in the formation of a MgO-MnO solid solution. The brick installed in the furnace bottom was additionally infiltrated with FeMn.
- The copper cooling elements in the furnace bottom and the slag zone resulted in a very steep thermal gradient in the brick lining. The refractory material was therefore exposed to significant thermal shocks that promoted crack formation and spalling.

The furnace operation results and refractory investigations demonstrated that the novel Alloysstream™ process and furnace type, as well as the use of a non-carbon lining, is technically feasible for HCFeMn production, and an interesting alternative to the standard FeMn SAF process.

ACKNOWLEDGEMENTS

The authors would like to acknowledge the valuable contributions of Thomas Prietl and Steyn Theron, which were deeply involved in the lining

design and material optimization, as well as acted as an indispensable link between RHI Austria and Exxaro Alloystream™.

REFERENCES

1. S.E. Olsen, M. Tangstad, and T. Lindstad, *Production of Manganese Ferroalloys*, 1st ed. (Trondheim: SINTEF and Tapir Academic Press, 2007), pp. 43–50.
2. T. Coetsee, C. Reinke, J. Nell, and P.C. Pistorius, *Metall. Mater. Trans. B* 46B, 2534 (2015).
3. M. Eissa, H. El-Faramawy, A. Ahmed, S. Nabil, and H. Halfa, *J. Miner. Mater. Charact. Eng.* 11, 1 (2012).
4. J. Madias, *A Review of the Production of Ferromanganese in Blast Furnace*, *AISTech Proceedings*, vol. 1 (USA: Indianapolis, 2011), pp. 401–412.
5. L.J. Fourie, US patent 6,146,437 (2000).
6. M. Gasik, *Handbook of Ferroalloys—Theory and Technology*, 1st ed. (Oxford: Butterworth-Heinemann, 2013), pp. 238–249.
7. M. Tangstad and S.E. Olsen, *The Ferromanganese Process—Material and Energy Balance* (Trondheim, Norway: INFACON, 1995), pp. 621–630.
8. T. Coetsee, J. Muller, J.A. Groenewald, A.A du Toit, and D. Zeelie, *The Alloystream™ Process for HCFeMn Production* (Kiev, Ukraine: INFACON, 2014), pp. 91–98.
9. D. Gregurek, A. Ressler, V. Reiter, A. Franzkowiak, A. Spanring, and T. Prietl, *JOM* 65, 1622 (2013).
10. U. Hyungsic, L. Kyuyong, J. Choi, and Y. Chung, *ISIJ Int.* 52, 62 (2012).
11. L.R. Nelson and R.J. Hunermark, *The Tap-Hole—Key to Furnace Performance* (Johannesburg, South Africa: The SAIMM Furnace Tapping Conference, 2014), pp. 1–32.
12. J. Muller, J.H. Zietsman, and P.C. Pistorius, *Metall. Mater. Trans. B* 46B, 2639 (2015).
13. G. Routschka, *Refractory Materials*, 4th ed. (Essen: Vulkan-Verlag, 2011), p. 505.
14. M. Rigaud, *Uhlig's Corrosion Handbook*, ed. R.W. Revie (Hoboken, NJ: Wiley, 2011), p. 385.
15. C. Wenzl and A. Spanring, *RHI Refractory Solutions—A Reliable Partner for the Ferroalloys Industry* (Kiev, Ukraine: INFACON, 2015), pp. 264–269.
16. S. Luidold, H. Schneideritsch, and H. Antrekowitsch, *Berg-Huettenmaenn Monatsh Suppl.* 156, 1 (2011).
17. D. Gregurek, C. Wenzl, V. Reiter, H.L. Studnicka, and A. Spanring, *JOM* 66, 1677 (2014).
18. W.A. Deer, R.A. Howie, and J. Zussman, *An Introduction to the Rock-Forming Minerals*, 2nd ed. (UK: Essex CM20 2 JE, 1992), pp. 108–177.
19. C.W. Bale, P. Chartrand, S.A. Deckerov, G. Eriksson, K. Hack, R. Ben Mahfoud, J. Melançon, A.D. Pelton, and S. Petersen, *Calphad* 62, 189 (2002).